Geomorphology 246 (2015) 35–47

Contents lists available at ScienceDirect

Geomorphology

journal homepage: www.elsevier.com/locate/geomorph

Potential of two submontane broadleaved species (*Acer opalus*, *Quercus pubescens*) to reveal spatiotemporal patterns of rockfall activity

Adrien Favillier [a], Jérôme Lopez-Saez [b], Christophe Corona [c,*], Daniel Trappmann [d], David Toe [b], Markus Stoffel [d,e,f], Georges Rovéra [a], Frédéric Berger [b]

[a] Institut de Géographie Alpine, Laboratoire Politique publiques, Action Politique, Territoire (PACTE) UMR 5194 du CNRS, Université Joseph Fourier, 14 bis avenue Marie Reynoard, 38100 Grenoble, France
[b] Institut national de Recherche en Sciences et Technologies pour l'Environnement et l'Agriculture (IRSTEA), UR EMGR, 38402 St-Martin-d'Hères cedex, France
[c] UMR6042 Geolab, Université Blaise Pascal, 4 rue Ledru, F-63057 Clermont-Ferrand, France
[d] Dendrolab.ch, Institute of Geological Sciences, University of Berne, Baltzerstrasse 1 + 3, CH-3012 Berne, Switzerland
[e] Section of Earth and Environmental Sciences, University of Geneva, rue des Maraîchers 13, CH-1205 Geneva, Switzerland
[f] Institute for Environmental Sciences, University of Geneva, 7 route de Drize, CH-1227 Carouge, Geneva, Switzerland

ARTICLE INFO

Article history:
Received 26 November 2014
Received in revised form 4 June 2015
Accepted 5 June 2015
Available online 8 June 2015

Keywords:
Forest–rockfall interactions
Coppice stands
Dendrogeomorphology
Recurrence intervals
Submontane broadleaved species
French Alps

ABSTRACT

Long-term records of rockfalls have proven to be scarce and typically incomplete, especially in increasingly urbanized areas where inventories are largely absent and the risk associated with rockfall events rises proportionally with urbanization. On forested slopes, tree-ring analyses may help to fill this gap, as they have been demonstrated to provide annually-resolved data on past rockfall activity over long periods. Yet, the reconstruction of rockfall chronologies has been hampered in the past by the paucity of studies that include broadleaved tree species, which are, in fact, quite common in various rockfall-prone environments. In this study, we test the sensitivity of two common, yet unstudied, broadleaved species — *Quercus pubescens* Willd. (*Qp*) and *Acer opalus* Mill. (*Ao*) — to record rockfall impacts. The approach is based on a systematic mapping of trees and the counting of visible scars on the stem surface of both species. Data are presented from a site in the Vercors massif (French Alps) where rocks are frequently detached from Valanginian limestone and marl cliffs. We compare recurrence interval maps obtained from both species and from two different sets of tree structures (i.e., single trees vs. coppice stands) based on Cohen's *k* coefficient and the mean absolute error. A total of 1230 scars were observed on the stem surface of 847 *A. opalus* and *Q. pubescens* trees. Both methods yield comparable results on the spatial distribution of relative rockfall activity with similar downslope decreasing recurrence intervals. Yet recurrence intervals vary significantly according to tree species and tree structure. The recurrence interval observed on the stem surface of *Q. pubescens* exceeds that of *A. opalus* by >20 years in the lower part of the studied plot. Similarly, the recurrence interval map derived from *A. opalus* coppice stands, dominant at the stand scale, does not exhibit a clear spatial pattern. Differences between species may be explained by the bark thickness of *Q. pubescens*, which has been demonstrated to grow at twice the rate of *A. opalus*, thus constituting a mechanical barrier that is able to buffer low energy rockfalls and thus can avoid damage to the underlying tissues. The reasons for differences between tree structures are related to the clustered coppice-specific spatial stem distribution in clumps that could result on one hand in bigger gaps between clumps, which in turn decreases the probability of tree impacts for traveling blocks. On the other hand, data also indicate that several scars on the bark of coppice stands may stem from the same impact and thus may lead to an overestimation of rockfall activity.

1. Introduction

Rockfall is defined as the free-falling, bouncing, or rolling of rocks originating from cliff faces with a volume usually remaining below 5 m^3 (Berger et al., 2002; Dorren et al., 2005). It is a common and dangerous natural process in steep environments that can lead to important economic losses and casualties (e.g., Hantz et al., 2003). In principle, rockfall hazard can be defined as the probability that a specific location on a slope is reached by a rockfall of a given magnitude (Volkwein et al., 2011). The frequency of events of a given magnitude (volume) can be evaluated using a statistical analysis of inventories of rockfall events (e.g., Hungr et al., 1999), taking into account the definition of suitable magnitude–frequency relationships (e.g., Dussauge-Peisser et al., 2002). Although this approach is well established in the field of natural hazards, and in particular for earthquakes, its application to rockfall

* Corresponding author.
E-mail address: christophe.corona@univ-bpclermont.fr (C. Corona).

http://dx.doi.org/10.1016/j.geomorph.2015.06.010
0169-555X/

hazards is somewhat more limited because of the generalized lack of historical archives and the spatial and temporal heterogeneity of available inventories (e.g., Sass and Oberlechner, 2012).

If talus slopes or the runout fringe of boulders beyond the talus foot are covered with forests, individual rockfall fragments may damage or even destroy trees along their trajectory (Stoffel, 2006; Trappmann et al., 2014). Woody vegetation damaged by rockfalls or growing on talus thus provides a valuable means for dating and interpreting past rockfalls with high accuracy and over long periods of the past (Stoffel et al., 2010; Šilhán et al., 2011). Dendrogeomorphic methods (Alestalo, 1971; Shroder, 1978; Stoffel and Corona, 2014) aim at inferring data on past processes from information preserved in tree rings. Previous tree-ring studies primarily focused on rockfall damage in conifers for the reconstruction of rockfall frequencies (Stoffel et al., 2005a,b; Perret et al., 2006b), the spatial distribution and magnitude of rockfalls (Stoffel et al., 2005b), the triggering of rockfalls by climatic variables (Schneuwly and Stoffel, 2008; Šilhán et al., 2011) as well as on the comparison of observed and/or reconstructed rockfall inventories with activity predicted by three-dimensional, process-based rockfall models (Stoffel et al., 2006; Corona et al., 2013). Occasionally but very rarely, rockfall research has included broadleaved trees growing on talus slopes to document recent activity (Moya et al., 2010a; Šilhán et al., 2011; Trappmann and Stoffel, 2013), mainly owing to a complex wood structure of broadleaved species that rendered tree-ring analysis challenging in the absence of specific anatomical responses (Arbellay et al., 2012, 2014a,b). The preferred sampling of conifers over broadleaved trees was, in addition, motivated by the greater age and the predominance of conifers in mountain regions where rockfalls typically occur.

This selective approach and related gap in knowledge is regrettable for three characteristics typical for broadleaved species: (i) they are typically predominant at altitudes belonging to the sub-montane belt where rockfalls threaten infrastructure and structures much more frequently than at higher altitudes (Sass and Oberlechner, 2012); (ii) broadleaved trees typically have a thin and smooth bark structure that not only facilitates wounding but also enhances the visibility of scars on the stem surface (Stoffel, 2005; Stoffel and Perret, 2006); and (iii) the particular bark structure renders broadleaved species highly suitable for scar counts on the stem surface, but the approach has only been tested on *Fagus sylvatica* L. (common beech) trees to date (Trappmann and Stoffel, 2013).

The primary objective of this study therefore was to test the sensitivity of two common, yet unstudied, broadleaved species, *Quercus pubescens* (*Qp*) and *Acer opalus* (*Ao*), to rockfall impacts. Furthermore, this study explores the influence of bark thickness and structure on recorded rockfall frequency by comparing results obtained with a smooth (*Ao*) and a thick (*Qp*) barked species. Results were gathered through an exhaustive mapping of 847 *Ao* and *Qp* trees from a 0.6-ha plot and are based on 1230 scars visible on the tree stem surface as well as on bark thickness measurements. We demonstrate that rockfall patterns

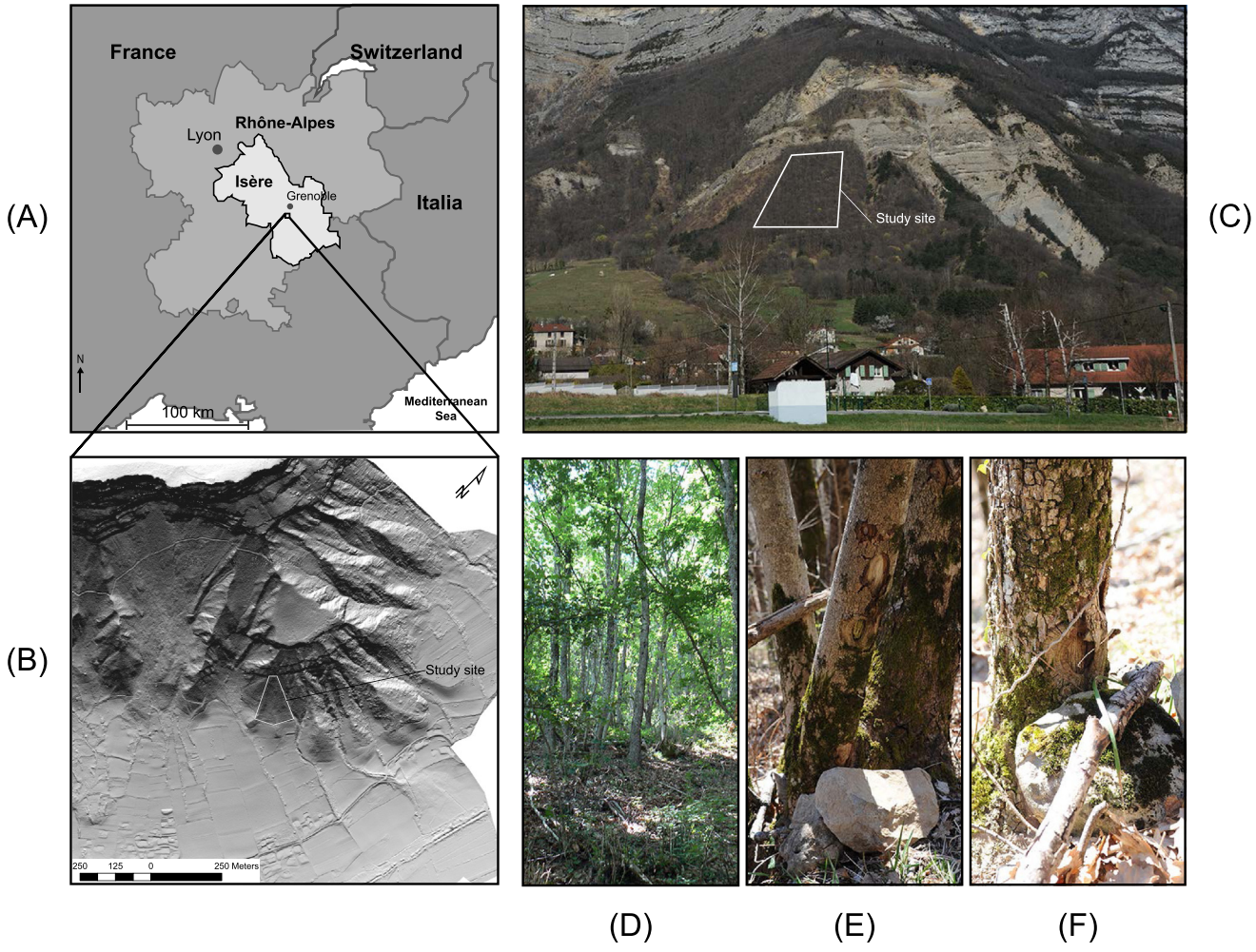

Fig. 1. (A) The study site is located in the French Alps, at the eastern face of the Vercors massif, 20 km southwest of Grenoble. (B) Hillshade map computed using the DEM derived from airborne LiDAR data with the study site delimited by a white polygon. View of studied slope (C), the forest stand (D), injured *Acer opalus* (E), and *Quercus pubescens* stems (F).

derived from both species vary considerably, especially in the lower part of the studied plot, primarily as a result of differences in bark thickness.

2. Study site

The study site (45°05′02″N, 5°39′16″E) is located on the eastern slope of the Vercors massif (French Alps; Fig. 1A and B), in the vicinity of Saint-Paul-de-Varces (2500 people), and at a locality known under the name of "Croupe du Plantin". The elevation of the studied slope ranges from 470 to 630 m asl. Rockfall originates from an ~30-m-high, south east-facing cliff built of Valanginian limestones and marls where a narrow joint system favors considerable fragmentation and the release of small rock fragments with volumes ranging from a few dm^3 to 1 m^3 (Hantz et al., 2014). According to the high-resolution DEM derived from airborne LiDAR data, Quaternary rockfalls have formed a ~240-m-long talus slope with a downslope gradient ranging from 39° to 25° (Fig. 2B) that is bordered by two interfluves (Fig. 2A). At the apex of the talus, slope morphology is characterized by a slight depression (depth ~2 m) that splits into two ~30-m-wide couloirs that channelize falling rock fragments downslope (Fig. 2D and E).

The tree plot analyzed here has an area of 0.6 ha and is covered by a dense (~2000 trees ha^{-1}) coppice forest stand (Fig. 1C and D) predominantly composed of *Ao* and *Qp* mixed with *Sorbus aria* (L.) Crantz (common whitebeam), *Acer campestre* L. (field maple), and *Fraxinus excelsior* L. (common ash). Frequent scars on the stem surface clearly evidence the presence of regular rockfall activity (Fig. 1E and

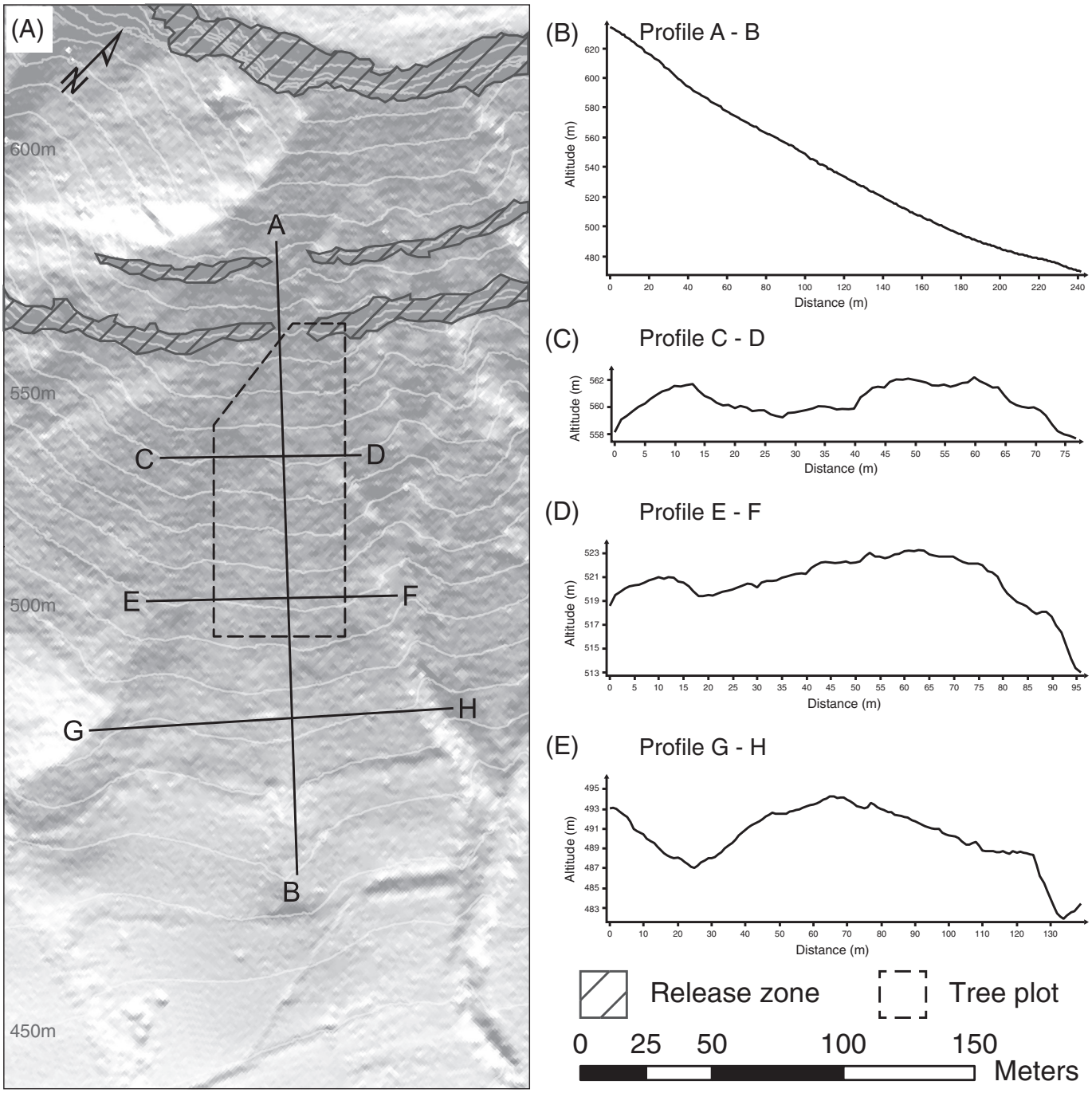

Fig. 2. (A) Hillshade map of the study site. (B) Longitudinal and (C, D, E) lateral profiles of the studied slope.

F). Mean annual precipitation (1961–2013) at the nearest meteorological station, Grenoble (45°09′58″N, 5°45′58″E, 220 m asl), located 10 km northeast of the study site is 934 mm year^{-1}. Mean annual temperature is 12.5 °C with 64 days year^{-1} experiencing freezing. Rock fragments are dislodged from the cliff along preexisting or new discontinuities and the triggering mechanisms of rockfalls include freeze–thaw cycles of interstitial water (Matsuoka and Sakai, 1999) as well as intense rainfall (Cardinali et al., 2006).

The municipality of Saint-Paul de Varces is severely exposed to rockfall hazards. Two major collapses can be found in historical archives, one at the beginning of the seventeenth century and another one in December 2008, with the latter having a volume estimated to 1625 m^3 (Hantz et al., 2014). Vulnerability of the settlement to rockfall has increased rapidly since the 1950s owing to the rapid periurban expansion in the wider Grenoble region (Astrade et al., 2007). As a consequence, rockfall hazard assessment is primarily of importance for local stakeholders and policy makers.

3. Material and methods

In this study, two different broadleaved species, *A. opalus* and *Q. pubescens* have been used to assess past rockfall activity. The "Croupe du Plantin" tree plot was selected as (i) both species are present at the same site and almost evenly distributed, (ii) past rockfalls have left numerous visible impacts on tree stems (Fig. 1E and F), and (iii) no other geomorphic processes caused injuries to trees. On this slope, the recorded rockfall frequency was evaluated with a five-step procedure including the (i) scar-counting approach on a tree sample plot, (ii) assessment of tree age based on age–diameter regression models (Rozas, 2003), (iii) computation of individual recurrence intervals of rockfalls at the level of individual trees, and (iv) the comparison of results for each species based on the mean absolute error (MAE) and the Cohen's kappa coefficient. In a final step, (v) the influence of bark on the recurrence intervals computed from each species was investigated through bark thickness measurements and bark structural analyses.

3.1. Tree plot and scar-counting approach

At the study site, virtually all trees show visible growth anomalies on the stem surface resulting from past rockfalls, predominantly in the form of injuries. As scars represent the most accurate and reliable growth disturbance (GD) to date past rockfalls in tree-ring records (Stoffel, 2005; Schneuwly and Stoffel, 2008; Schneuwly et al., 2009), we actively searched for visible stem wounds. To precisely assess the spatial and temporal patterns of past rockfall activity, trees with a diameter at breast height (DBH) > 5 cm were systematically mapped in a 50 × 120 m tree plot orientated perpendicular to the line of maximum slope gradient (Fig. 3). The position of each tree was determined (±100 cm) using a sonic rangefinder, compass, and inclinometer. Tree species as well as information on tree structure (single stem vs. coppice stands), which likely have an impact on the mechanical behavior of the tree (Jancke, 2012), were recorded as well. All trees were positioned in a geographical information system (GIS; Kennedy, 2009; ESRI, 2012) as geo-objects.

Trappmann and Stoffel (2013) have previously demonstrated the reliability of the scar-counting approach to reconstruct spatial patterns of rockfall activity. We therefore employed this method as well in a second step as it requires much less time and effort to estimate the rockfall frequency at the level of individual trees from the plot than conventional dendrogeomorphic approaches. The latter is time-consuming as it requires an exhaustive sampling (cross sections and cores), identifications and dating of growth reaction that formed after mechanical disturbances caused by rock impacts (see Trappmann and Stoffel, 2013, for more details). Recent scars were identified according to their fresh appearance, chipped bark, or injured wood (see Trappmann and Stoffel., 2015, for details). Presently overgrowing wounds were identified based on the callus pad that is sealing the injuries from the border toward the center (Stoffel and Perret, 2006). Older, completely healed injuries are more difficult to be detected visually; they were inferred via the occurrence of swelling and blisters on the stem surface. Extremely long, vertical scars or scars with vertical extensions of <3 cm were excluded from analysis so as to avoid misclassification and/or the inclusion of injuries caused by branch breakage (Perret et al., 2006a).

3.2. Development of age–diameter regression models

In a second step, linear diameter–age regression models (Rozas, 2003) were built for *Ao* and *Qp*. For that purpose, a total of 90 undisturbed trees (41 *Qp*, 49 *Ao*) with a DBH ≥ 10 cm were cored using a Pressler increment borer. Trees were selected according to five diameter classes, representative of the tree plot, and discriminated between single trees and coppice stands. The samples were analyzed and data

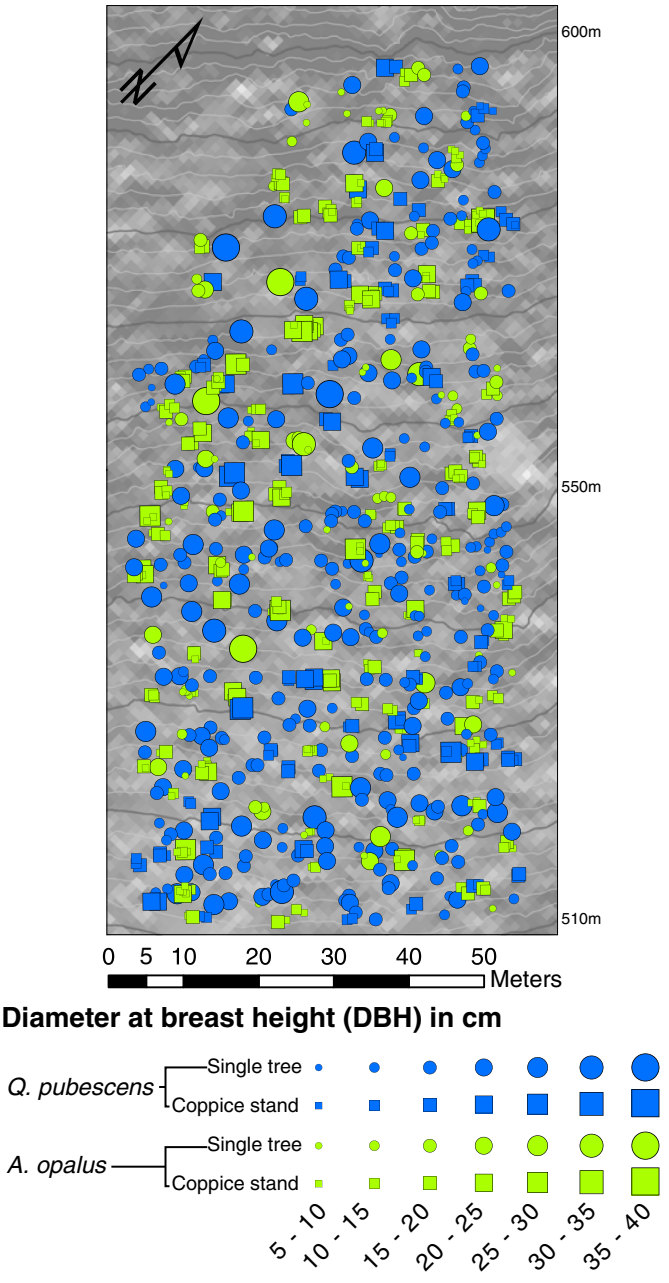

Fig. 3. Spatial distribution and diameters at breast height (DBH; in cm) of *Quercus pubescens* and *Acer opalus* in the studied tree plots.

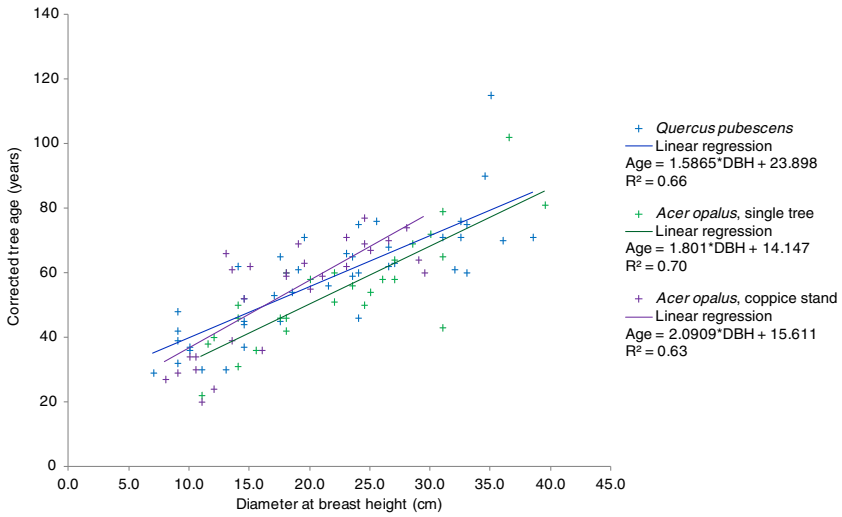

Fig. 4. Age–diameter regression models for *Quercus pubescens* and *Acer opalus*.

processed following standard dendrochronological procedures (Bräker, 2002). In the laboratory, tree rings were counted using a digital LINTAB positioning table connected to a Leica stereomicroscope. Missing rings toward the pith were estimated from ring curvature (Villalba and Veblen, 1997). In a final step, we used data from the linear regression models to estimate tree age of individual trees of the plot where scars were counted on the stem surface and the DBH has been measured.

3.3. Calculation of rockfall recurrence intervals

The term *recurrence interval* has been used traditionally in avalanche zoning (e.g., Schläppy et al., 2014) and only started to occur in rockfall studies over the past few years (Šilhán et al., 2013; Trappmann et al., 2013);it is defined as the average time period between two successive events at a specific point (or tree). Individual recurrence intervals (Ri) were calculated for each tree T and following Šilhán et al. (2013) as:

$$Ri_T = A_T Sc_T \tag{1}$$

where A_T represents the age of tree T estimated from age–diameter models (Fig. 4) and Sc_T the number of scars counted on the stem surface of tree T.

To visualize spatial patterns of recurrence intervals and to remove potential outliers, trees were clustered into 10 × 10 m cells ($n = 54$). For each cell C, the average recurrence interval Ri_c was computed as the arithmetic mean of Ri_T of trees (N_T: the number of trees) located in C as:

$$Ri_C = \left(\sum Ri_T\right)/N_T. \tag{2}$$

At each cell, a total of five different Ri_c involving all trees, *Ao*, *Qp*, single stems, and coppice stands were successively computed.

3.4. Comparison of Ao and Qp recurrence intervals

At the tree plot scale, the Cohen's kappa coefficient (Smeeton, 1985) was computed to compare the similarity of maps derived from *Ao* and *Qp* trees. Cohen's kappa (k) measures the agreement between two raters (species in our case) that each classify N items (cells) into C mutually exclusive categories (classes of recurrence intervals) as:

$$k = \frac{\Pr(a)/\Pr(e)}{1-\Pr(e)} \tag{3}$$

where $\Pr(a)$ is the relative observed agreement among species, and $\Pr(e)$ is the hypothetical probability of chance agreement, using the observed data to calculate the probabilities of each species distributed randomly in each class of recurrence interval. According to Landis and Koch (1977), k values < 0 indicate no agreement, 0–0.20 slight, 0.21–0.40 fair, 0.41–0.60 moderate, 0.61–0.80 substantial, and 0.81–1 almost perfect agreement.

At the cell scale, the mean absolute error (MAE) was computed for each cell c containing both species (Corona et al., 2013; Trappmann and Stoffel, 2013) for three pairs of maps (including all morphologies, single stem, and coppice stand) as:

$$MAE_c = Ri_c(Qp) - Ri_c(Ao) \tag{4}$$

where $Ri_c(Qp)$ and $Ri_c(Ao)$ represent the mean recurrence interval of rockfalls computed from *Qp* and *Ao* in cell c. Results from Eq. (3) were accepted if MAE_c remained within the range of ±10 years (the sign ± is used here to indicate 1 standard deviation).

Table 1
Overview of scars and calculated recurrence interval for *Quercus pubescens* and *Acer opalus* single trees and coppice stands.

Species	No. of trees	Mean DBH in cm (STD)	Mean age in year (SD)	Sum of scars	Mean number of scars per tree (SD)	Mean recurrence interval in year
Quercus pubescens	441 (52.1%)	17.6 (5.9)	52 (9.4)	601	1.4 (1.8)	41.00
Single tree	309 (36.5%)	18.0 (6.1)	53 (9.7)	420	1.4 (1.7)	41.00
Coppice stand	132 (15.6%)	16.6 (5.5)	50 (8.8)	181	1.4 (1.9)	40.00
Acer opalus	406 (47.9%)	17.6 (6.1)	42 (12.3)	629	1.5 (2.1)	32.00
Single tree	94 (11.1%)	14.5 (6.8)	40 (12.2)	173	1.8 (2.6)	29.00
Coppice stand	312 (36.8%)	12.8 (5.9)	42 (12.3)	456	1.5 (2.0)	33.00
Total	847 (100%)	15.5 (6)	41 (11.6)	1230	1.5 (2.0)	37

3.5. Bark thickness analysis

Trappmann and Stoffel (2013) suggested that bark structure and the genetic capability of trees to overgrow injuries could explain the variations in the mean number of impacts recorded by *Picea abies* L. and *F. sylvatica* L. In a final step, in order to assess the influence of bark on reconstructed *Ri*, the bark thickness of 102 *Qp* and *Ao* selected according to five diameter classes, representative of the tree plot, was recorded using a Suunto bark gauge with a precision of 1 mm (West, 2009). At the same time, the DBH of each tree was recorded using a Zimmer

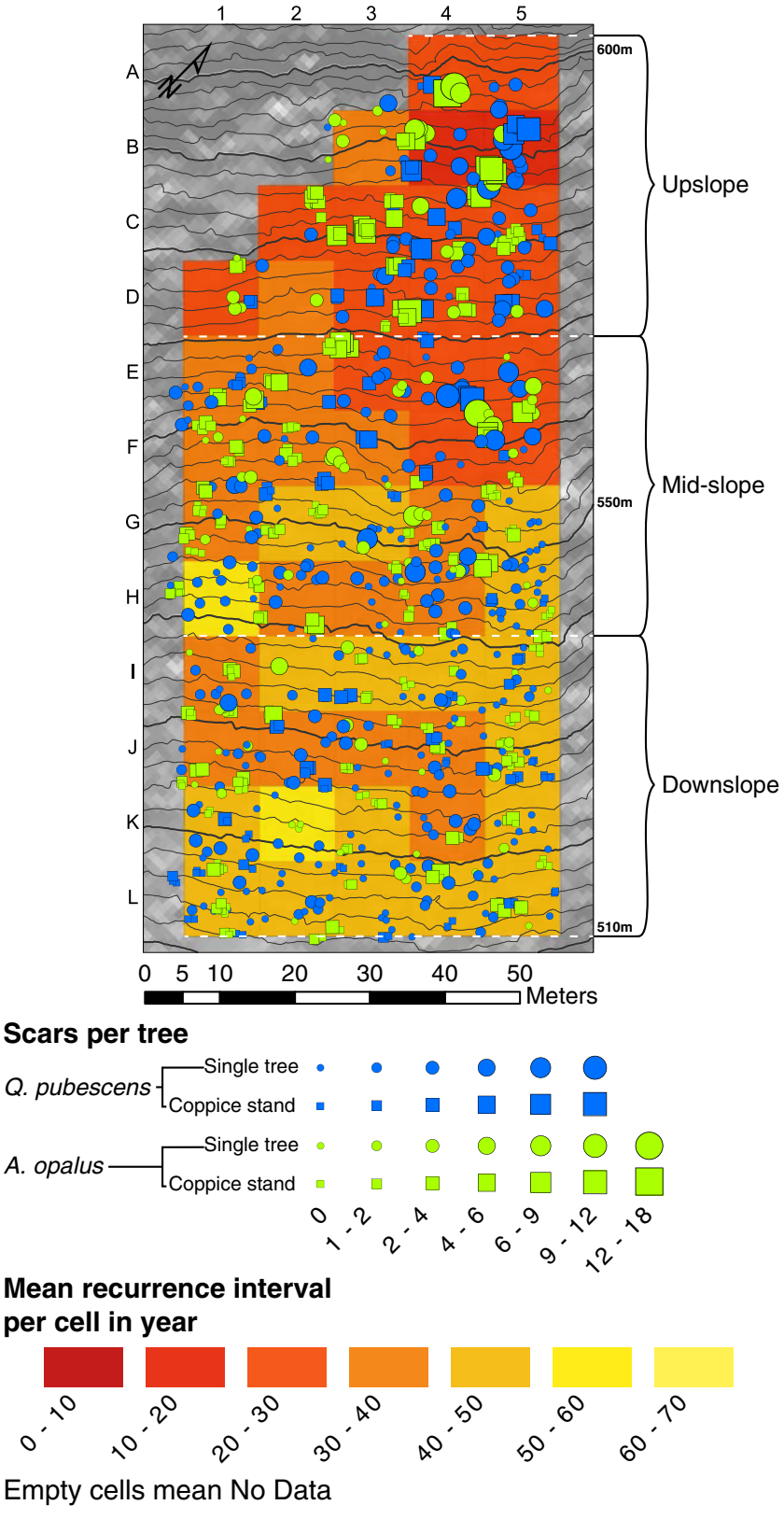

Fig. 5. Reference recurrence interval map (Refmap) calculated for 847 single trees and coppice stands.

diameter tape. Additionally, wedges were extracted from 8 trees, 4 *Qp* (*Qp*1–*Qp*4) and 4 *Ao* (*Ao*1–*Ao*4) of different DBHs (7.5–39 cm). Wedges were scanned at a resolution of 1200 dpi to characterize the main anatomical differences between both species (Quilhó et al., 2013).

4. Results

4.1. Structure of the forest plot: a mixed A. opalus–Q. pubescens forest stand

At the plot scale, a total of 847 trees were mapped (mean DBH: 15.5 ± 6.0 cm) among which 441 *Qp* (52.1%, mean DBH: 17.6 ± 5.9 cm) and 406 *Ao* (47.9%, mean DBH: 13.2 ± 6.1 cm) trees (see Table 1 for a complete description) were heterogeneously distributed in the cells (Figs. 3 and 5). In terms of morphology, the plot is composed of 403 single stems (47.6%), mainly *Qp* trees (77%), and 444 coppice stands with a majority of *Ao* trees (70%).

The regression models established for both species and tree structures are statistically significant (r^2 ranging between 0.63 and 0.7, $p < 0.05$) with comparable regression slopes (from 1.6 to 2.1 cm year^{-1}), thus enabling derivation of reliable tree ages from tree diameters (Fig. 4). According to these models, the mean age of the forest stand, computed from 847 mapped trees, is 41 ± 11.6 years. The oldest tree reached breast height 86 years ago while the youngest one was only 23 years old at the time of field analyses.

4.2. Spatiotemporal patterns of rockfall activity

Based on the scar-counting approach, 1230 scars were recorded on the stem surfaces (Table 1, Fig. 5). The mean number of scars per tree is 1.5 ± 2.0. A total of 309 trees (36%) present no visual evidence of past rockfall impacts. From a spatial perspective, the distribution of impacted trees exhibits a strong, decreasing downward gradient (Fig. 5). The mean number of scars revealed by the scar-counting approach gradually decreases from 3 ± 2.7 scars·tree^{-1} in the upper one-third of the slope (cells A–D) to 1.5 ± 1.8 scars·tree^{-1} in the central compartment of the plot (cells D–H) to reach values of 0.7 ± 0.9 in the lower one-third of the plot (cells I–L). Similarly, the largest absolute number of impacts (>9 scars) was mainly recorded in the upper half of the plot (A–F, Fig. 5) whereas the number of stems without impacts steadily increases from 23 (13%) in the upper one-third of the plot to 178 (54%) in its lower one-third. According to the linear regression models established for *Ao* and *Qp*, trees were aged 46.4 ± 11.7, 47 ± 11.6, and 47 ± 11.7 years in the upper, central, and lower one-thirds of the plot, respectively. In contrast to rockfall activity, no clear trend was discernible with respect to tree age.

Coupling the longitudinal gradient of impacts with the random distribution of tree ages results in a clear spatial downward trend of recurrence intervals (*Ri*) from <20 years in the upper part of the plot (A–F, Fig. 5, min < 10 years in cells B4 and B5) to >40 years in the lower cells (G–L, max > 60 years in cell K2). With respect to lateral spread, the *Ri* reference map derived from 847 trees (Refmap, Fig. 5) shows two preferential rockfall paths from E1 to K1 and from E4 to L4, which is in good agreement with the topographic depressions existing in the field. Several nonwounded trees in cells H3 to L2 and L3 are located on the interfluves, which is separating the aforementioned rockfall couloirs (Fig. 2C–E).

4.3. Influence of tree species on the reconstructed patterns

Scars recorded on the stem surface are almost equally distributed in terms of frequency between *Qp* (601, mean: 1.4 ± 1.8 scars·tree^{-1}) and *Ao* (629, mean: 1.5 ± 2.1 scars·tree^{-1}; Table 1) with maxima per sampled tree of 11 and 17 and comparable downslope gradients (3 ± 65 scars·tree^{-1} for *Qp*, 3.2 ± 75 scars·tree^{-1} for *Ao*, Table 2) between the species. On average, *Qp* trees are, however, slightly older (52 ± 9.4 years) than *Ao* trees (42 ± 12.3 years).

At the tree plot scale, the *Ri*(*Qp*) value (41 years) exceeds that of *Ri*(*Ao*) (32 years) by 9 years. The *Ri*(*Qp*) map (Fig. 6A) can be separated roughly into three parallel stripes (A–F, G–J, K–L) of increasing *Ri*, ranging from 10 to 20 years in the upper stripe to >60 years at the lower portions of the plot. A bimodal pattern is observed on the *Ri*(*Ao*) map (Fig. 6B) with an $Ri_c(Ao) < 20$ years in 19 out of 23 cells in half of the upper part of the slope (A–E) and an $Ri_c(Ao) > 30$ years in 90% of the cells located below 550 m asl (H–L). The *k* coefficient reaches 0.08 and thus reveals a slight agreement between maps obtained for either species.

The numbers of scars as observed in individual trees can vary significantly within the same sector as a result of the small-scale variability of rockfall processes. Nevertheless, a comparison of both approaches on the basis of grid cells as presented in Fig. 6C suggests that variation between both species is acceptable in 27 out of 53 cells. Cells where *Qp* yields higher Ri_c are located in the upper one-third of the slope (D2, E4, F1) and mainly reflect small (D2) or different interspecies sample sizes (E4). Conversely, cells where *Ao* yields higher Ri_c are scattered

Table 2
Age of trees and number of scars divided in three slope compartments. Downslope represents the lower third part, mid-slope the central part and upslope the upper third part of the slope.

Species	Area	Number of trees (unimpacted trees in %)	Scars per tree				Age of tree		
			Min	Max	Mean (SD)	Sum	Min	Max	Mean (SD)
All morphologies (single stem + coppice stand)	Downslope	329 (54.1%)	0	5	0.69 (0.9)	228	23.7	81.7	47.0 (11.7)
	Mid-slope	320 (33.8%)	0	14	1.48 (1.8)	472	23.1	79.9	47.4 (11.6)
	Upslope	170 (13.5%)	0	17	3.00 (2.7)	510	24.1	86.4	46.4 (11.6)
Acer opalus	Downslope	140 (52.8%)	0	5	0.75 (1.0)	105	23.7	81.7	39.7 (12.6)
	Mid-slope	163 (33.1%)	0	14	1.45 (1.8)	236	23.1	79.9	43.5 (12.8)
	Upslope	89 (13.5%)	0	17	3.17 (3.0)	282	24.1	80.8	42.0 (12.0)
Single tree	Downslope	32 (53.1%)	0	5	0.78 (1.1)	25	23.7	81.7	40.5 (13.9)
	Mid-slope	39 (25.6%)	0	14	1.95 (2.6)	76	23.1	79.8	38.7 (14.5)
	Upslope	20 (10.0%)	0	16	3.55 (3.3)	71	24.1	80.2	43.4 (13.6)
Coppice stand	Downslope	108 (52.8%)	0	4	0.74 (1.0)	80	26.1	74.6	39.4 (12.2)
	Mid-slope	124 (35.5%)	0	7	1.29 (1.5)	160	26.1	72.7	45.0 (11.8)
	Upslope	69 (14.5%)	0	17	3.06 (2.9)	211	26.5	80.8	41.7 (11.5)
Quercus pubescens	Downslope	189 (55.0%)	0	4	0.65 (0.9)	123	33.7	78.8	52.3 (7.3)
	Mid-slope	157 (34.9%)	0	11	1.50 (1.8)	236	35.8	79.5	51.3 (8.3)
	Upslope	81 (13.6%)	0	11	2.82 (2.3)	228	33.1	86.4	51.1 (9.1)
Single tree	Downslope	131 (51.1%)	0	4	0.69 (0.8)	90	33.7	78.8	53.1 (7.3)
	Mid-slope	122 (35.2%)	0	11	1.48 (1.8)	180	35.8	79.4	51.6 (8.6)
	Upslope	47 (10.6%)	0	11	2.94 (2.1)	138	40.2	86.4	52.7 (10.3)
Coppice stand	Downslope	58 (63.8%)	0	3	0.57 (0.9)	33	39.8	68.5	50.6 (6.8)
	Mid-slope	35 (31.4%)	0	11	1.60 (2.0)	56	40.1	69.9	51.3 (7.6)
	Upslope	34 (17.6%)	0	10	2.65 (2.4)	90	33.1	58.8	48.9 (6.3)

throughout the plot (23 cells out of 54) with maximal differences (>40 years) observed in its lowest part (J, K, L).

4.4. Influence of tree structure on reconstructed patterns

Distinction between single stems and coppice stands allows investigation of the influence of tree structure on *Ri* maps. Comparable statistical results are obtained for both species (Table 1) with respect to the mean number of scars per tree, whereas tree age and *Ri* are ~10 years higher in *Qp* (in terms of single stems and of coppice stands) than in *Ao* trees. Interspecies comparison (Table 3) also reveals major differences ($k < 0$) in results between *Ri* maps derived from single stems (Fig. 7A, B) mainly resulting from lower *Ri*(*Ao*) values, especially in the lowest part of the slope (K–L, Fig. 7C). Similarly, a slight agreement is observed between the *Ri* maps computed from coppice stands (Fig. 8A, B) resulting from cells where *Ao* yields higher Ri_c scattered throughout the plot (Fig. 8C). Conversely, however, intraspecies comparisons are characterized by higher degrees of similarity (k ranging between 0.31 and 0.7). Finally, the k coefficient reveals that *Ri* maps obtained from *Qp* and coppice stands of *Ao* are in fair agreement (k ~0.3) with the Refmap and should be preferred to *Ao* single stems for which a complete absence of agreement (~ −0.02) was obtained (Table 3).

4.5. Bark thickness analysis

To assess the influence of bark thickness on reconstructed recurrence intervals from both species, a total of 102 trees selected according to five diameter classes representative of the tree plot (Table 4), have been gauged. The mean bark thickness of sampled *Qp* was 14 ± 4.0 mm (min: 8 mm, max: 24 mm) for *Ao* and 4 ± 2.1 mm (min: 1 mm, max: 10 mm) for *Ao*. The regression bark thickness models established for both species and tree morphologies are statistically significant ($r^2(Qp) = 0.55$, $r^2(Ao) = 0.77$, Fig. 9A). The regression slopes

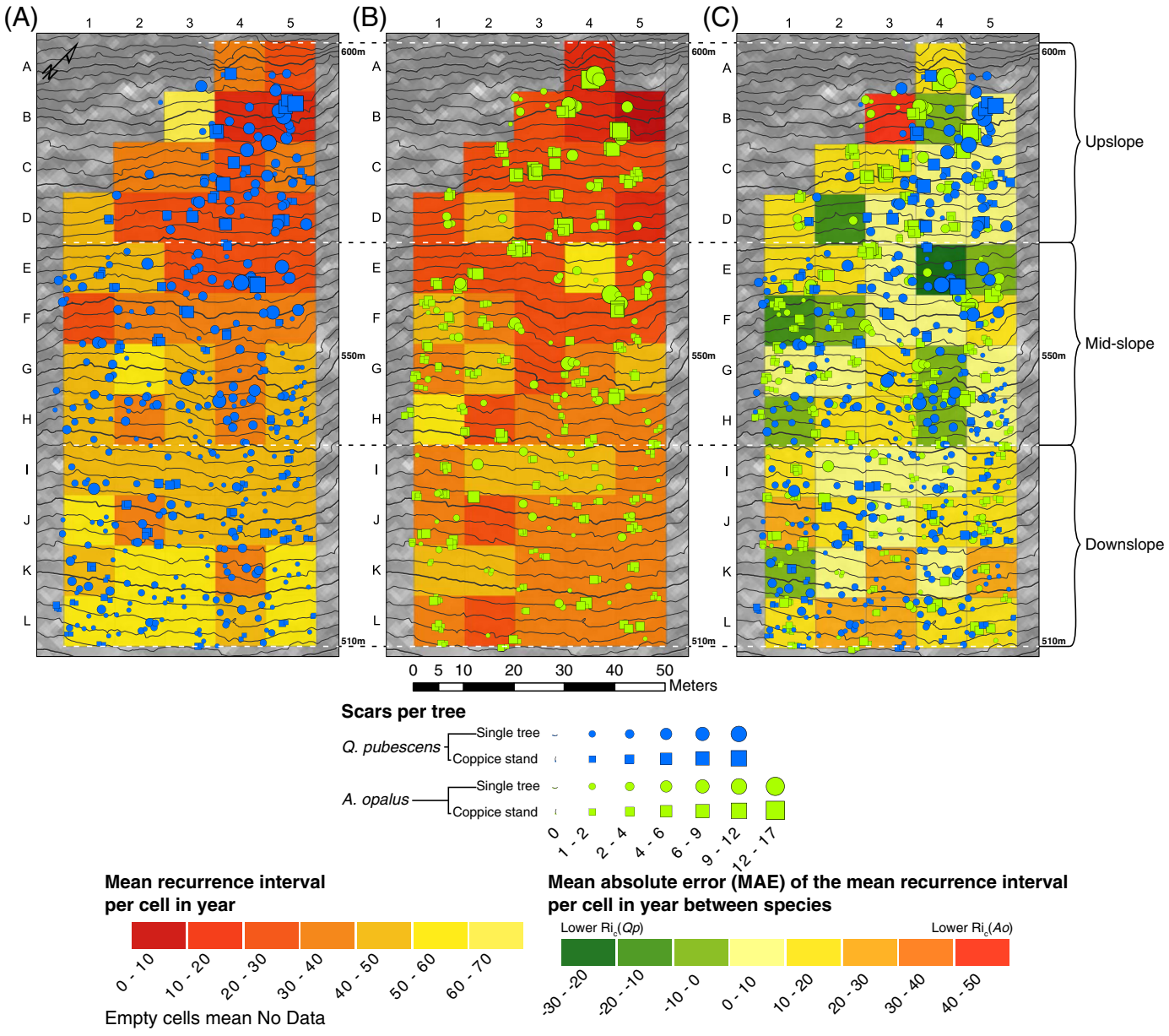

Fig. 6. Recurrence interval map (Refmap) calculated for (A) *Quercus pubescens*, (B) *Acer opalus* trees and (C) variations of the recurrence interval between species.

Table 3
Cohen's kappa coefficient test computed between recurrence interval maps derived from single stems, coppice stands and both tree morphologies for the two species, Ao and Qr.

		Single tree		Coppice stand		All morphologies (single stem + coppice stand)		
		Ao	*Qp*	*Ao*	*Qp*	*Ao*	*Qp*	Refmap (*Ao* + *Qp*)
Single tree	*Ao*							
	Qp	−0.0284						
Coppice stand	*Ao*	0.0345	0.0671					
	Qp	0.0276	0.167	0.0477				
All morphologies (single stem + coppice stand)	*Ao*	0.306	0.11	0.577	0.0808			
	Qp	−0.0618	0.704	0.0426	0.393	0.0829		
	Refmap (*Ao* + *Qp*)	−0.0189	0.311	0.289	0.261	0.376	0.358	

(0.44 cm year^{-1} for *Qp*, 0.2 cm year^{-1} for *Ao*) reveal that the bark of *Qp* grows at twice the rate as compared to that of *Ao*. Similarly, bark thickness of *Qp* is more than twice as important as that of *Ao*, independently of diameter class. For example, for an ~20-cm-diameter tree, the maximum bark thickness of *Ao* ranges between 2 and 5 mm, while the minimum bark thickness of *Qp* is always >10 mm. Similarly, for an ~30-cm tree, the maximum bark thickness of *Ao* is 6 mm, while the minimum bark thickness of *Qp* is 15 mm.

In addition, anatomical analyses of the sampled wedges clearly demonstrated that the two species under investigation are characterized by different bark structures: the overall structure of *Qp* bark is rough and thick and contains a pyramidal outer structure (also known as rhytidome), whereas the bark of *Ao* is thin and comparably smooth. The bark samples, *Qp*3 and *Ao*1, shown in Fig. 9, clearly illustrate these differences: *Qp*3 (Fig. 9B, diam: 31.4 cm) has a 17.5-mm-thick bark composed of a 4.7-mm-thick phloem (inner bark), a 1.9-mm-thick

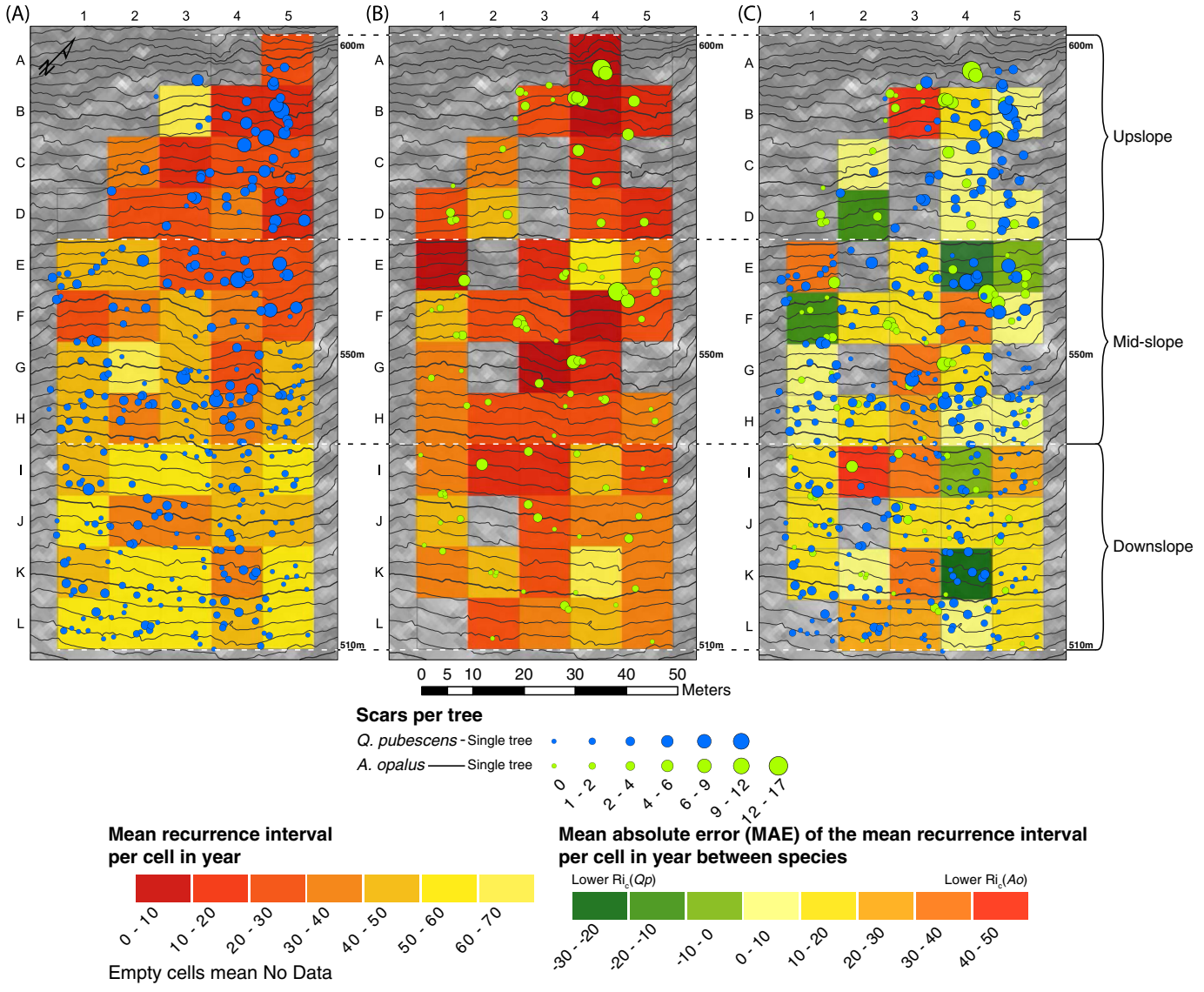

Fig. 7. Recurrence interval map calculated for *Quercus pubescens* (A), *Acer opalus* (B) single trees and (C) variations of the recurrence interval.

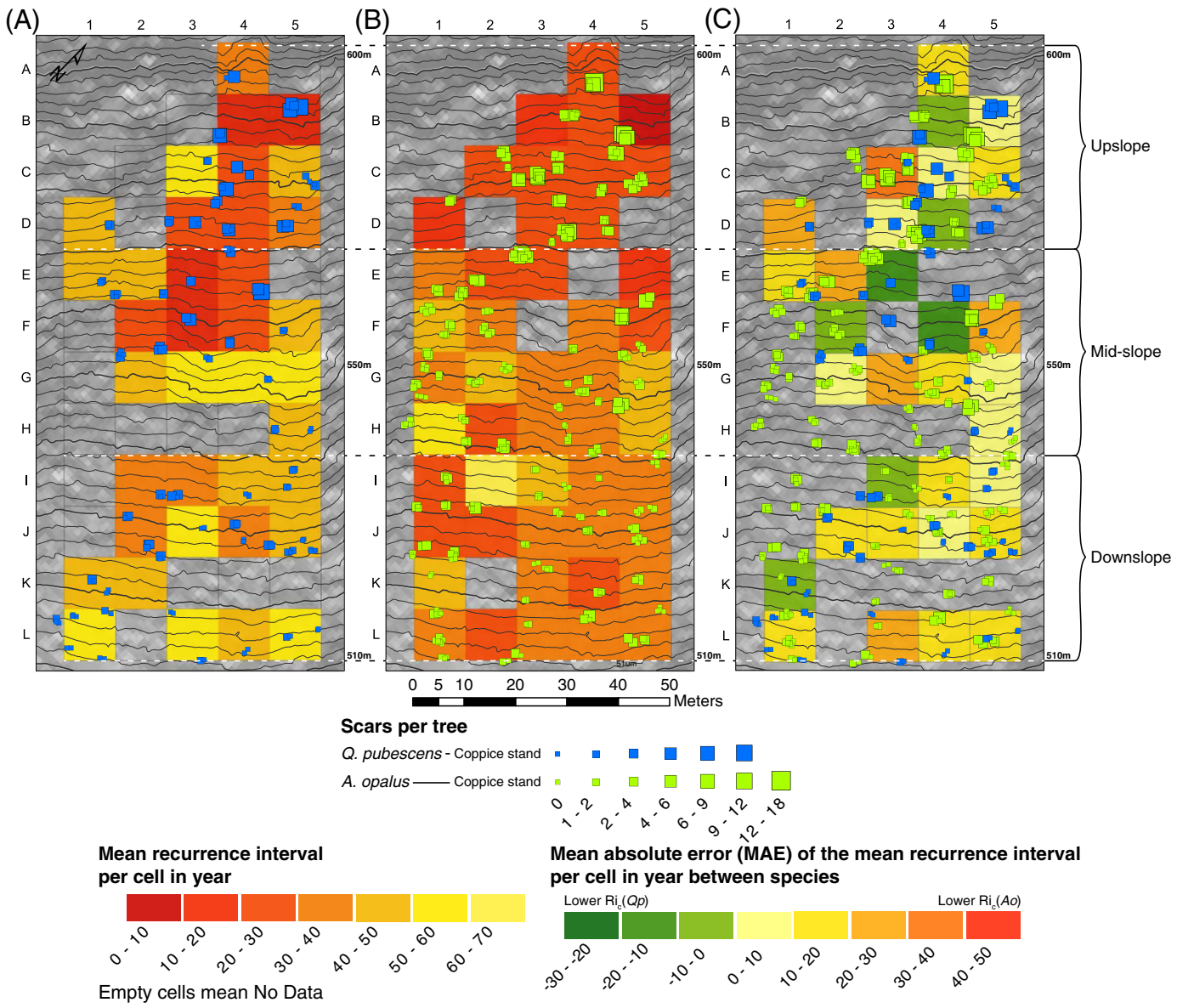

Fig. 8. Recurrence interval maps calculated for *Quercus pubescens* (A), *Acer opalus* (B) coppice stands and (C) variations of the recurrence interval.

periderm (central bark), and a 10.8-mm-thick rhytidome (outer bark). Conversely, *Ao*1 (Fig. 9C, diam: 28.3 cm) has a 5.5-mm-thick bark composed of three distinct layers: a 3.9-mm-thick phloem, a 1-mm-thick periderm and a 0.6-mm-wide cork.

5. Discussion

Long-term records of rapid mass movements, such as rockfalls, have proven to be quite limited, especially in urbanized areas where inventories are largely absent (Volkwein et al., 2011) and where, at the same time, the number of events increases in proportion to urbanization (Baillifard et al., 2004). In these areas, finding ways that allow precise reconstruction of past rockfall activity are urgently needed. In case such slopes are forested, dendrogeomorphology is a reliable alternative that allows one to reconstruct past rockfall activity in the absence of any inventory or clear morphological evidence, such as scree slopes or isolated blocks (Volkwein et al., 2011). Yet with a few exceptions (Moya et al., 2010a; Šilhán et al., 2011; Trappmann and Stoffel, 2013), broadleaved trees did not receive much attention in tree-ring reconstructions and even less so at the submontane level where urbanization is often most pronounced. In the study presented here, we tested the robustness and dendrogeomorphic potential of two broadleaved species, *Q. pubescens* (*Qp*) and *A. opalus* (*Ao*) (Csaikl et al., 2002; Tissier et al., 2004) with the aim of (i) assessing the robustness of these species to reconstruct past rockfall activity for several decades and (ii) testing the influence of tree species and bark thickness and structure on the reconstructed spatial and temporal patterns of rockfalls. The selection of the species was motivated by their widespread occurrence on low-altitude (<900 m asl), south-facing slopes in the Alps.

Based on an exhaustive mapping of 847 *Ao* and *Qp* trees and the systematic counting (Trappmann et al., 2013) of 1230 visible scars on tree stems in a 0.6-ha plot, our study demonstrates a marked downslope

Table 4
Overview of *Quercus pubescens* and *Acer opalus* bark thickness analyses.

Species	No. of trees	Mean DBH in cm (SD)	Mean bark thickness in mm (SD)
Quercus pubescens	50	22.0 (6.7)	14 (4.0)
Acer opalus	52	19.0 (9.2)	4 (2.1)
Total	102	20.5 (8.3)	

decrease in the number of observed scars per stem in both species. The related upslope-decreasing recurrence intervals (*Ri*) also clearly demonstrate the protective effect of the forest at the study site. Recurrence intervals are consistent with the concave profile of the slope and further highlight the energy absorption of rockfalls (i) at each impact point, especially for the first ones (Evans and Hungr, 1993) and (ii) through

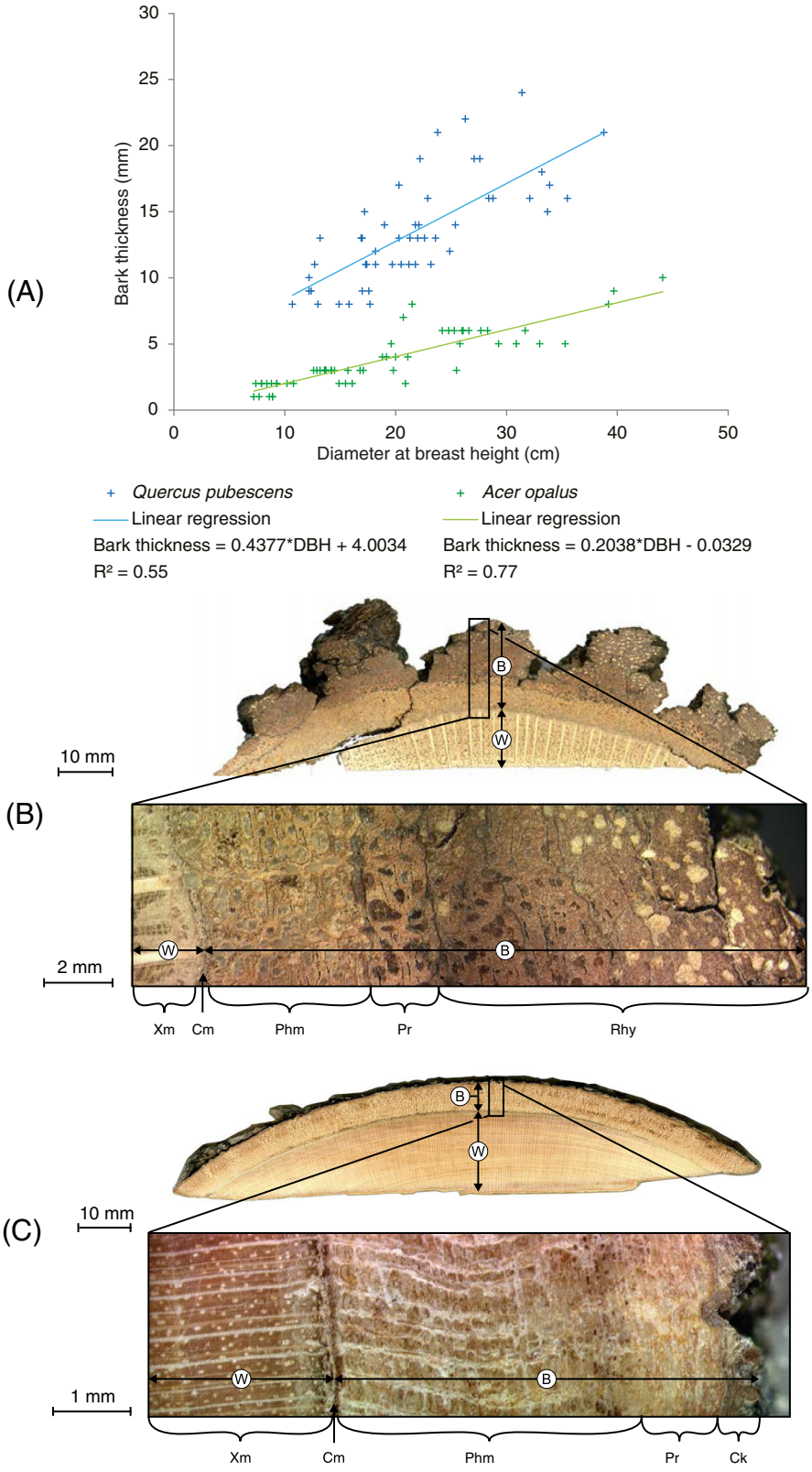

Fig. 9. Bark analysis for *Quercus pubescens* and *Acer opalus*. (A) Bark thickness–diameter linear regression models. (B) Details of *Quercus pubescens* (wedge section *Qp*3) and (C) *Acer opalus* (wedge section *Ao*1). B: bark; W: wood; Xm: xylem; Cm: cambium; Phm: phloem; Pr: periderm; Rhy: rhytidome; Ck: cork. *Qp*3 has a DBH of 31.4 cm and a gauged bark thickness of 24 mm. *Ao*1 has a DBH of 28.3 cm and a gauged bark thickness of 6 mm.

direct impact between a boulder and a trunk (e.g., Gsteiger, 1989; Dorren et al., 2005, 2006). In addition, lower recurrence intervals are also observed in topographic depressions, where rockfall tends to be channelized. Besides the pure recording of impacts stemming from past rockfall activity, we also confirm the ability of *Ao* and *Qp* to integrate and thus represent morphologic constraints of the rockfall path (Nicoletti and Sorriso-Valvo, 1991; Corominas, 1996).

While both species yield comparable downslope patterns of decreasing rockfall activity along the slope, they also exhibit a series of differences in the absolute numbers of events recorded on the stem surfaces and hence in the return intervals obtained from *Ao* and *Qp* at the cell scale. As a result, while yielding the same mean number of scars (1.5 scars stem^{-1}), *Ao* produces recurrence intervals that are, in 40% of the cells, more than 10 years smaller than those observed in *Qp*, therefore resulting in only slight agreement if maps are obtained separately for each species. We attribute (part of) these differences between *Ao* and *Qp* to species-specific differences in bark structure and thickness. Indeed, rockfall wounding only occurs if a falling block is able to abrade the bark and to (partly) destroy the underlying cambium (Stoffel and Bollschweiler, 2008). In that case, tree growth will be disrupted locally, therefore leading to the formation of externally visible wound callus pads (Larson, 1994; Fink, 1999). As a consequence, only those rockfalls with sufficient energy to mechanically damage cambium (Schneuwly, 2009) will leave evidence on the stem, whereas the impact of small rock fragments may not necessarily be recorded by a tree. In this study, we demonstrate that the bark of *Qp* thickens at twice the rate of that of *Ao* and that bark thickness of *Qp* was more than twice as important as compared to *Ao* for a same-diameter class. These differences are interpreted as different adaptation strategies — e.g., heat-protecting function in the case of the thick and fissured *Qp* bark or, by contrast, energy saving and limited allocation of resources to bark formation in pioneering plants such as *Ao* so as to remain competitive during the colonization process (Nicolai, 1986) — and may have led to different sensitivities of trees to be injured by mechanical impacts. Taking into account the rather limited volume of rocks at "Croupe du Plantin" (0.06 m^3 for the biggest fragments), we believe that the thicker outer bark found in *Qp* could indeed act as a mechanical barrier to damage (Fritts, 1976), thereby buffering low energy rockfalls and avoiding injury of the underlying tissues. Moreover, the flexible pyramidal outer bark of *Qp* may, in addition, be very well able to comply with mechanical stress (Romero, 2006). On the other hand, impacts of similar energy may be sufficient to cause injury to the softer and coated xylem of *Ao*, which is only poorly protected from damage by a very thin bark. This hypothesis is consistent with the increasing downslope differences and quasi-systematic overestimation of recurrence intervals in *Qp*, especially in the lower one-third of the slope where the residual energy of rocks will be limited as a result of multiple rebounds and interactions with stems higher up on the slope.

A second reason for the interspecies differences is certainly related to the effect of hidden scars (Stoffel and Perret, 2006). Indeed, surface exposed to decay as a result of wounding will slowly be covered by the centripetal growth of the cambium, which will consequently result in the production of new wood and bark tissues that can eventually seal the wound (Fisher, 1981; Sachs, 1991). The extent and velocity of wound healing will depend on various factors, such as the annual increment rate, tree age, health state of the tree, scar size (Bollschweiler et al., 2008; Schneuwly et al., 2009), and/or bark thickness (Stoffel and Perret, 2006). Stoffel (2005), for instance, could identify 75% of all scars by visual interpretation through the simple inspection of the bark structure of *F. sylvatica*, whereas only 51% of the injuries remained visible on the stem surface of *P. abies*. Similarly, on a mixed forest stand in the Austrian Alps, Trappmann and Stoffel (2013) observed that the mean number of scars on the stem surface of *F. sylvatica* exceeded that of *P. abies* by a factor of 2.7 and for the same site. In analogy with these results, one can assume that virtually all scars would remain visible on the stem surface of *Ao*, whereas wound blurring could indeed remove evidence of past events on the stem surface of *Qp* owing to its thicker and rougher bark.

Additionally, reasons for differences at the cell scale can be related to the clustered coppice-specific spatial stem distribution in clumps. At the scale of individual trees, the effect of an impact upon a group of stump shoots of a coppiced tree is not necessarily the same as that of a similar impact on a noncoppiced plant of equivalent diameter (Jancke et al., 2009). As clumps consist of a dense bundle of stems with relatively small diameters, one single boulder passing through a cluster would likely hit several stems and might thus leave multiple scars (Ciabocco et al., 2009). Yet this phenomenon depends on the volume of the block. If the boulder is small, the likelihood for it to pass through the coppice shoots of the same stump will be larger than in the case of a larger stump (Trappmann et al., 2013; Morel et al., 2015). This phenomenon is further amplified when boulders bounce higher; so that they cross the coppice shoots at greater height, where the distance between trunks naturally increases. Using the scar count approach, each injury on a clump is considered as an individual rockfall that might result in an overestimation of real frequencies (Trappmann and Stoffel, 2013). This hypothesis is further supported by the *Ri* map computed from coppice stands, especially from *Ao* stumps dominant in the study plot, which yield lower recurrence intervals throughout the slope. We therefore feel that scars located very close to each other should not be considered as individual events in future studies or to include impact probability concepts (Moya et al., 2010b; Trappmann et al., 2014) to reduce the bias introduced by multiple impacts.

6. Conclusion

The findings of this study indicate quite clearly that an assessment of rockfall activity based on visible damage on *A. opalus* and *Q. pubescens* trees will result at the slope scale in similar data on the spatial distribution of relative rockfall activity with similar downslope-decreasing recurrence intervals. Yet the recurrence intervals observed on the stem surface of *Q. pubescens* exceed that of *A. opalus* by >20 years in the lower part of the plot owing to the thicker bark of *Qp* that constitutes an efficient mechanical barrier buffering low energy rockfalls. Results also (i) suggest that the dendrogeomorphic reconstruction of past rockfalls is more accurate if analyses are performed using a sampling design mixing species and structures and (ii) confirm the reliability of the counting scar approach as an efficient and effective method for the spatial assessment of rockfall activity on larger surfaces, as it can be realized with limited temporal and financial efforts. Despite the differences in rockfall recurrence intervals computed for each of the tree species, *A. opalus* and *Q. pubescens* proved to be valuable sources of information for the reconstruction of former events at Saint-Paul-de-Varces. They should be used more widely in future tree-ring studies, especially because they typically colonize low-altitude slopes, close to urbanized areas, where conifers are generally absent.

Acknowledgments

This work has been supported by a grant LabEx Osug@2020 (Investissements d'avenir — ANR10LABX56). The authors are grateful to Eric Mermin, Pascal Tardif, Franck Bourrier, Rémi Rosamont, Jordan Fèvre and all of the IRSTEA team Mountain Ecosystems for their scientific and technical supports and helpful comments. The authors acknowledge the three anonymous reviewers for their helpful comments on the manuscript and to Richard A. Marston for the thorough editing.

References

Alestalo, J., 1971. Dendrochronological interpretation of geomorphic processes. Fennia 105, 1–139.
Arbellay, E., Fonti, P., Stoffel, M., 2012. Duration and extension of anatomical changes in wood structure after cambial injury. J. Exp. Bot. 63, 3271–3277.

Arbellay, E., Stoffel, M., Sutherland, E.K., Smith, K.T., Falk, D.A., 2014a. Resin duct size and density as ecophysiological traits in fire scars of *Pseudotsuga menziesii* and *Larix occidentalis*. Ann. Bot. 114, 973–980. http://dx.doi.org/10.1093/aob/mcu168.

Arbellay, E., Stoffel, M., Sutherland, E.K., Smith, K.T., Falk, D.A., 2014b. Changes in tracheid and ray traits in fire scars of North American conifers and their ecophysiological implications. Ann. Bot. 114, 223–232. http://dx.doi.org/10.1093/aob/mcu112.

Astrade, L., Lutoff, C., Nedjai, R., Philippe, C., Loison, D., Bottollier-Depois, S., 2007. Periurbanisation and natural hazards. J. Alp. Res. 95, 19–28. http://dx.doi.org/10.4000/rga.132.

Baillifard, F., Jaboyedoff, M., Rouiller, J.D., Robichaud, G.R., Locat, P., Locat, J., Couture, R., Hamel, G., 2004. Towards a GIS-based hazard assessment along the Quebec City Promontory, Quebec, Canada. In: Lacerda, W.A., Ehrlich, M., Fontoura, S.A.B., Sayao, A.S.F. (Eds.), Landslides: Evaluation and Stabilization. Taylor & Francis Group, London, pp. 207–214.

Berger, F., Quetel, C., Dorren, L.K.A., 2002. Forest: A Natural Protection Mean Against Rockfalls, but With Which Efficiency. Int. Congr. Interpraevent.

Bollschweiler, M., Stoffel, M., Schneuwly, D.M., Bourqui, K., 2008. Traumatic resin ducts in *Larix decidua* stems impacted by debris flows. Tree Physiol. 28, 255–263. http://dx.doi.org/10.1093/treephys/28.2.255.

Bräker, O.U., 2002. Measuring and data processing in tree-ring research — a methodological introduction. Dendrochronologia 20, 203–216.

Cardinali, M., Galli, M., Guzzetti, F., Ardizzone, F., Reichenbach, P., Bartoccini, P., 2006. Rainfall induced landslides in December 2004 in south-western Umbria, central Italy: types, extent, damage and risk assessment. Nat. Hazards Earth Syst. Sci. 6, 237–260.

Ciabocco, G., Boccia, L., Ripa, M.N., 2009. Energy dissipation of rockfalls by coppice structures. Nat. Hazards Earth Syst. Sci. 9, 993–1001.

Corominas, J., 1996. The angle of reach as a mobility index for small and large landslides. Can. Geotech. J. 33, 260–271.

Corona, C., Trappmann, D., Stoffel, M., 2013. Parameterization of rockfall source areas and magnitudes with ecological recorders: when disturbances in trees serve the calibration and validation of simulation runs. Geomorphology 202, 33–42. http://dx.doi.org/10.1016/j.geomorph.2013.02.001.

Csaikl, U.M., Burg, K., Fineschi, S., König, A.O., Mátyás, G., Petit, R.J., 2002. Chloroplast DNA variation of white oaks in the Alpine region. For. Ecol. Manag. 156, 131–145.

Dorren, L.K.A., Berger, F., le Hir, C., Mermin, E., Tardif, P., 2005. Mechanisms, effects and management implications of rockfall in forests. For. Ecol. Manag. 215, 183–195.

Dorren, L.K.A., Berger, F., Putters, U.S., 2006. Real-size experiments and 3-D simulation of rockfall on forested and non-forested slopes. Nat. Hazards Earth Syst. Sci. 6, 145–153.

Dussauge-Peisser, C., Helmstetter, A., Grasso, J.-R., Hantz, D., Desvarreux, P., Jeannin, M., Giraud, A., 2002. Probabilistic approach to rock fall hazard assessment: potential of historical data analysis. Nat. Hazards Earth Syst. Sci. 2, 15–26.

ESRI 2012. ArcGIS 10.1 for desktop. Redlands, CA.

Evans, S.G., Hungr, O., 1993. The assessment of rockfall hazard at the base of talus slopes. Can. Geotech. J. 30, 620–636.

Fink, S., 1999. Pathological and Regenerative Plant Anatomy, in: Encyclopedia of Plant Anatomy. Gebrüder Bornträger, Berlin, Stuttgart.

Fisher, J.B., 1981. Wound-healing by exposed secondary xylem in *Adansonia* (Bombacaceae). IAWA Bull. 2, 193–199.

Fritts, H.C., 1976. Tree-rings and Climate. Academic Press, London.

Gsteiger, P., 1989. Steinschlag, Wald, Relief. Empirische Grundlagen zur Steinschlagmodellierung. Université de Bern, Bern, Suisse (Thèse non publiée).

Hantz, D., Vengeon, J.M., Dussauge-Peisser, C., 2003. An historical, geomechanical and probabilistic approach to rock-fall hazard assessment. Nat. Hazards Earth Syst. Sci. 3, 693–701.

Hantz, D., Rossetti, J., Servant, F., D'Amato, J., 2014. Etude de la distribution des blocs dans un éboulement pour l'évaluation de l'aléa. Presented at the Rock Slope Stability, Marrakech, Maroc, p. 10.

Hungr, O., Evans, S.G., Hazzard, J., 1999. Magnitude and frequency of rock falls and rock slides along the main transportation corridors of southwestern British Columbia. Can. Geotech. J. 36, 224–238.

Jancke, O., 2012. Quantifying the Mechanical Resistance of Coppice Trees Against Rockfall (Thesis). University of Hamburg, Hamburg.

Jancke, O., Dorren, L.K.A., Berger, F., Fuhr, M., Köhl, M., 2009. Implications of coppice stand characteristics on the rockfall protection function. For. Ecol. Manag. 259, 124–131. http://dx.doi.org/10.1016/j.foreco.2009.10.003.

Kennedy, M., 2009. Introducing Geographic Information Systems With ArcGIS: A Workbook Approach to Learning GIS. John Wiley & Sons.

Landis, J.R., Koch, G.G., 1977. The measurement of observer agreement for categorical data. Biometrics 33, 159–174.

Larson, P.R., 1994. The Vascular Cambium — Development and Structure. Springer, Berlin.

Matsuoka, N., Sakai, H., 1999. Rockfall activity from an alpine cliff during thawing periods. Geomorphology 28, 309–328.

Morel, P., Trappmann, D., Corona, C., Stoffel, M., 2015. Defining sample size and sampling strategy for dendrogeomorphic rockfall reconstructions. Geomorphology 236, 79–89.

Moya, J., Corominas, J., Arcas, J.P., 2010a. Assessment of the rockfall frequency for hazard analysis at Solà d'Andorra (Eastern Pyrenees). In: Stoffel, M., Bollschweiler, M., Butler, D.R., et al. (Eds.), Tree Rings and Natural Hazards. Springer, Dordrecht: Netherlands, pp. 161–175.

Moya, J., Corominas, J., Pérez Arcas, J., Baeza, C., 2010b. Tree-ring based assessment of rockfall frequency on talus slopes at Solà d'Andorra, Eastern Pyrenees. Geomorphology 118, 393–408. http://dx.doi.org/10.1016/j.geomorph.2010.02.007.

Nicolai, V., 1986. The bark of trees: thermal properties, microclimate and fauna. Oecologia 69, 148–160.

Nicoletti, P.G., Sorriso-Valvo, M., 1991. Geomorphic controls of the shape and mobility of rock avalanches. Geol. Soc. Am. Bull. 103, 1365–1373.

Perret, S., Baumgartner, M., Kienholz, H., 2006a. Inventory and analysis of tree injuries in a rockfall-damaged forest stand. Eur. J. For. Res. 125, 101–110.

Perret, S., Stoffel, M., Kienholz, H., 2006b. Spatial and temporal rockfall activity in a forest stand in the Swiss preAlps — a dendrogeomorphological case study. Geomorphology 74, 219–231.

Quilhó, T., Sousa, V., Tavares, F., Pereira, H., 2013. Bark anatomy and cell size variation in *Quercus faginea*. Turk. J. Bot. 37, 561–570.

Romero, C., 2006. Tree Responses to Stem Damage (PhD). Florida.

Rozas, V., 2003. Tree age estimates in *Fagus sylvatica* and *Quercus robur*: testing previous and improved methods. Plant Ecol. 167, 193–212.

Sachs, T., 1991. Pattern Formation in Plant Tissue. Cambridge University Press, Cambridge.

Sass, O., Oberlechner, M., 2012. Is climate change causing increased rockfall frequency in Austria? Nat. Hazards Earth Syst. Sci. 12, 3209–3216. http://dx.doi.org/10.5194/nhess-12-3209-2012.

Schläppy, R., Eckert, N., Jomelli, V., Stoffel, M., Grancher, D., Brunstein, D., Naaim, M., Deschatres, M., 2014. Validation of extreme snow avalanches and related return periods derived from a statistical–dynamical model using tree-ring techniques. Cold Reg. Sci. Technol. 99, 12–26. http://dx.doi.org/10.1016/j.coldregions.2013.12.001.

Schneuwly, D.M., 2009. Tree Rings and Rockfall — Anatomic Tree Reactions and Spatio-temporal Rockfall Analysis (Geoscience). Fribourg, Fribourg, Suisse.

Schneuwly, D.M., Stoffel, M., 2008. Tree-ring based reconstruction of the seasonal timing, major events and origins of rockfall on a case study slope in the Swiss Alps. Nat. Hazards Earth Syst. Sci. 8, 203–211.

Schneuwly, D.M., Stoffel, M., Dorren, L., Berger, F., 2009. Three-dimensional analysis of the anatomical growth response of European conifers to mechanical disturbance. Tree Physiol. 29, 1247–1257. http://dx.doi.org/10.1093/treephys/tpp056.

Shroder, J.F., 1978. Dendrogeomorphological analysis of mass movement on Table Cliffs Plateau, Utah. Quat. Res. 9, 168–185.

Šilhán, K., Brázdil, R., Pánek, T., Dobrovolný, P., Kašičková, L., Tolasz, R., Turský, O., Václavek, M., 2011. Evaluation of meteorological controls of reconstructed rockfall activity in the Czech Flysch Carpathians. Earth Surf. Proc. Land. 36, 1898–1909. http://dx.doi.org/10.1002/esp.2211.

Šilhán, K., Pánek, T., Hradecký, J., 2013. Implications of spatial distribution of rockfall reconstructed by dendrogeomorphological methods. Nat. Hazards Earth Syst. Sci. 13, 1817–1826. http://dx.doi.org/10.5194/nhess-13-1817-2013.

Smeeton, N.C., 1985. Early history of the kappa statistic. Biometrics 41, 795.

Stoffel, M., 2005. Assessing the vertical distribution and visibility of rockfall scars in trees. Schweiz. Z. Forstwes. 158, 195–199.

Stoffel, M., 2006. A review of studies dealing with tree rings and rockfall activity: the role of dendrogeomorphology in natural hazard research. Nat. Hazards 39, 51–70.

Stoffel, M., Bollschweiler, M., 2008. Tree-ring analysis in natural hazards research — an overview. Nat. Hazards Earth Syst. Sci. 8, 187–202.

Stoffel, M., Corona, C., 2014. Dendroecological dating of geomorphic disturbance in trees. Tree-Ring Res. 70, 3–20. http://dx.doi.org/10.3959/1536-1098-70.1.3.

Stoffel, M., Perret, S., 2006. Reconstructing past rockfall activity with tree rings: some methodological considerations. Dendrochronologia 24, 1–15.

Stoffel, M., Lièvre, I., Monbaron, M., Perret, S., 2005a. Seasonal timing of rockfall activity on a forested slope at Täschgufer (Valais, Swiss Alps) — a dendrochronological approach. Z. Geomorphol. 49, 89–106.

Stoffel, M., Schneuwly, D., Bollschweiler, M., Lièvre, I., Delaloye, R., Myint, M., Monbaron, M., 2005b. Analyzing rockfall activity (1600–2002) in a protection forest — a case study using dendrogeomorphology. Geomorphology 68, 224–241.

Stoffel, M., Wehrli, A., Kühne, R., Dorren, L.K.A., Perret, S., Kienholz, H., 2006. Assessing the protective effect of mountain forests against rockfall using a 3D simulation model. For. Ecol. Manag. 225, 113–122.

Stoffel, M., Schneuwly, D.M., Bollschweiler, M., 2010. Assessing rockfall activity in a mountain forest — implications for hazard assessment. In: Stoffel, M., Bollschweiler, M., Butler, D.R., Luckman, B.H. (Eds.), Tree Rings and Natural Hazards, Advances in Global Change Research. Springer, Netherlands, pp. 139–155.

Tissier, J., Lambs, L., Peltier, J.-P., Marigo, G., 2004. Relationships between hydraulic traits and habitat preference for six *Acer* species occurring in the French Alps. Ann. For. Sci. 61, 81–86.

Trappmann, D., Stoffel, M., 2013. Counting scars on tree stems to assess rockfall hazards: a low effort approach, but how reliable? Geomorphology 180, 180–186. http://dx.doi.org/10.1016/j.geomorph.2012.10.009.

Trappmann, D., Stoffel, M., 2015. Visual dating of rockfall scars in decidua trees. Geomorphology http://dx.doi.org/10.1016/j.geomorph.2015.04.030.

Trappmann, D., Corona, C., Stoffel, M., 2013. Rolling stones and tree rings: a state of research on dendrogeomorphic reconstructions of rockfall. Prog. Phys. Geogr. 37, 701–716. http://dx.doi.org/10.1177/0309133313506451.

Trappmann, D., Stoffel, M., Corona, C., 2014. Achieving a more realistic assessment of rockfall hazards by coupling three-dimensional process models and field-based tree-ring data. Earth Surf. Process. Landf. 39, 1866–1875. http://dx.doi.org/10.1002/esp.3580.

Villalba, R., Veblen, T.T., 1997. Improving estimates of total tree ages based on increment core samples. Ecoscience 4, 534–542.

Volkwein, A., Schellenberg, K., Labiouse, V., Agliardi, F., Berger, F., Bourrier, F., Dorren, L.K.A., Gerber, W., Jaboyedoff, M., 2011. Rockfall characterisation and structural protection — a review. Nat. Hazards Earth Syst. Sci. 11, 2617–2651. http://dx.doi.org/10.5194/nhess-11-2617-2011.

West, P.W., 2009. Tree and Forest Measurement. Springer Science & Business Media, Heidelberg.